Revista Mexicana de Astronomía y Astrofísica, **50**, 245–253 (2014)

THE COSMIC RAY AND THE 10.7 CM FLUX VARIATIONS DURING SOLAR CYCLES 19-23

J. E. Mendoza-Torres,[1] X. Luo,[2] and H. Salazar[3]

Received 2013 December 18; accepted 2014 April 30

RESUMEN

Estudiamos los flujos de rayos cósmicos (CRF) y de 10.7 cm (F10.7) para los ciclos solares 19-23. La correlación cruzada indica dependencia más prolongada en ciclos impares que en pares. El movimiento del máximo en los histogramas $CRF^1/F10.7^1$ (los cocientes de los valores normalizados), no depende de la polaridad del ciclo. El comportamiento de CRF^1 vs $F10.7^1$, difiere entre ciclos pares e impares y también en diferentes fases del ciclo. Ajustamos un perfil CRF^1 invertido (CRF^{inv}) a $F10.7^1$ con una función lineal. El histograma $F10.7^1/CRF^{inv}$ difiere para ciclos pares e impares. Los resultados para el número de manchas solares (SSN) son similares a los de F10.7 pero no para los histogramas $F10.7^1/SSN^{inv}$. Resumiendo, hay diferencias entre ciclos pares e impares, también en las fases de los ciclos y otras independientes de la polaridad del ciclo; estas últimas tal vez se originan fuera de la heliosfera.

ABSTRACT

The cosmic ray flux (CRF) and 10.7 cm flux (F10.7) are studied for solar cycles 19-23. The cross-correlations show longer time-dependence at odd than at even cycles. A shift of the maximum at the histograms of $CRF^1/F10.7^1$ (the ratios of normalized values), does not depend on the polarity of the cycle. The behavior of CRF^1 vs $F10.7^1$ differs for odd and even cycles and also for different cycle phases. We fitted an inverted CRF^1 profile to the $F10.7^1$ profile with a linear function. The $F10.7^1/CRF^{inv}$ histogram differs for odd and even cycles. The results for sunspot number (SSN) are similar to F10.7 but differ for the $F10.7^1/CRF^{inv}$ histograms. Summarizing, besides the differences between odd and even cycles, there occur variations at different phases of the cycles and also variations independent of the polarity of the cycle, the latter perhaps arising outside the heliosphere.

Key Words: Sun: activity — Sun: heliosphere — Sun: particle emission — Sun: radio radiation

1. INTRODUCTION

It is well known that the cosmic ray flux (further referred to as CRF) is modulated with the solar cycle of activity (Cliver & Ling 2001; Gupta et al. 2006). Modulation occurs mainly for galactic cosmic rays (GCR) which are of moderate energy. The CRF observed from Earth has been compared to the sunspot number (SSN) which is considered a standard indicator of activity (Usoskin et al. 2001; Heber et al. 2006). Also, there is a dependence of the CRF on the odd-even cycles. The running cross-correlation between CRF and SSN reaches the highest values, for odd cycles, at time-lags of a few months, while for even cycles at about one year (Singh et al. 2008; Usoskin et al. 2001).

Sunspots, seen in the photosphere, are a particular feature of active regions (AR) where a series of phenomena at different wavelengths are observed. Sunspots have been the most affordable feature for long-term observations.

At AR the enhanced microwave emission has been a good tool for diagnostics of plasma parameters, including the magnetic field (Aschwanden 2005). The flux at 10.7 cm (further referred to as F10.7) has been observed for several decades and has shown to be a good tracer of the solar cycle of activity. F10.7 arises at the AR at heights where magnetic fields could take values from a few hundred to about 1500 gauss (Akhmedov et al. 1982; Aschwanden 2005), which represents a large reservoir for the field ejected to the heliosphere. The F10.7 time series behaves similarly to the SSN one,

[1]Instituto Nacional de Astrofísica, Óptica y Electrónica, Puebla, Mexico.
[2]Center for Space Science and Applied Research, Beijing, China.
[3]Benemérita Universidad Autónoma de Puebla, Puebla, Mexico.

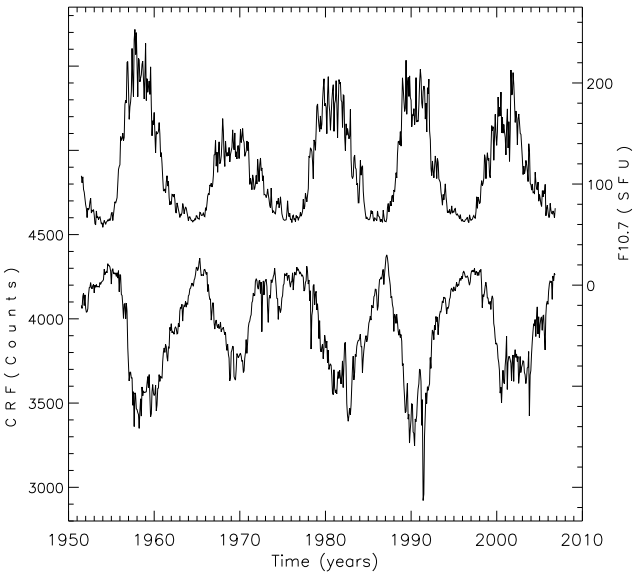

Fig. 1. Cosmic ray flux as observed at the Climax station and 10.7 cm flux observed at Penticton during solar cycles 19 to 23. The left scale corresponds to CR fluxes while the right one to F10.7

with some differences, among them being low values of SSN, which for monthly averages may be zero, while the smallest values of F10.7 are above 60 solar flux units (SFU), and, the variations of SSN at the high activity phase are larger than those at F10.7.

A sunspot forms when the underlying magnetic field is larger than a threshold value (Livingston et al. 2012). Even at regions with enhanced magnetic field, compared to the magnetic field of the quiet Sun, the photospheric region will not evolve to a sunspot, unless the magnetic field becomes larger than the threshold. As a result, at a given time, there could be several regions with enhanced magnetic field but if all of them are below the quoted value then the SSN will be zero. This means, the SSN is not sensitive to the appearance of regions with enhanced magnetic fields that do not exceed the threshold, even though there may be many such regions.

Microwave emission, whose origin is not clear, is observed even when SSN is zero. Part of the 10.7 cm remnant emission could be related to small scale and relatively weak magnetic fields. Since, as mentioned above, the F10.7 has some differences from SSN, we want to see if the relation between CRF and F10.7 is similar to that of CRF and SSN. The knowledge of these relations and in particular the recognition of similarities and differences with those observed between CRF and SSN would allow to identify how the F10.7 could contribute to the understanding of specific features of the modulation.

2. DATA ANALYSIS

For cosmic ray data the University of New Hampshire and the University of Bartol archives were used. The University of New Hampshire archive contains data of various stations with records from 1951, i.e. prior to cycle 19. The University of Bartol archive also includes records of various stations, some of them working from the early sixties, before cycle 20. The data consist of time series with several records per day. However, in some cases there are gaps with no observations, which last hours or even months. In the archive files these periods are filled with zeros. We averaged the CRF data over each month taking into account only observed values. For the Climax station of the New Hampshire archive, there are data from January 1951 and when computing the monthly averages up to 2006 there is only one gap in February 1951, i.e. before cycle 19. Climax data spans over cycles 19-23 (Figure 1). For McMurdo data at the Bartol archive there is only one gap for the monthly average which lies before cycle 20. Therefore, Climax data for the analysis of the 19-23 cycles and McMurdo data for the 20-23 cycles were used.

Penticton data for the 10.7 cm flux were used. These data are also time series of monthly averages recorded from 1947 with no gaps along cycles 19-23. Also, the monthly averages of the sunspot number were used. These data cover many solar cycles with no gaps for cycles 19-23.

To make data subsets according to the solar cycles, limits are taken at the activity minima which are 1954.25, 1964.75, 1976.42, 1986.67, 1996.33 and 2009.00. The published data of the Climax station contain records up to 2006. For this reason, in the analysis involving this station, the data of cycle 23 were taken until 2006. In this work we also use the maxima of the activity cycles which are taken at 1958.17, 1958.68, 1979.92, 1989.50.

2.1. *Running Cross-Correlations*

The running cross-correlation between CRF and F10.7 ($C_{CRF-F10.7}$) as well as for CRF and SSN ($C_{CRF-SSN}$) were estimated. As in previous reports, the behavior of the $C_{CRF-SSN}$ correlations differs for odd and even cycles. This is similar for $C_{CRF-F10.7}$ – a distinct behavior is observed between the cross-correlation for odd and even cycles. In Figure 2 the estimated $C_{CRF-F10.7}$ and $C_{CRF-SSN}$ values, using McMurdo data, are shown for time-lags up to 20 months. In Figure 3 the $C_{CRF-F10.7}$ for the five cycles, computed using Climax data, are shown. The behavior of the correlation using Climax and McMurdo data are similar.

The cross-correlation between CRF and F10.7 ($C_{CRF-F10.7}$) shows that for odd cycles the CRF variations remain correlated to F10.7 variations for

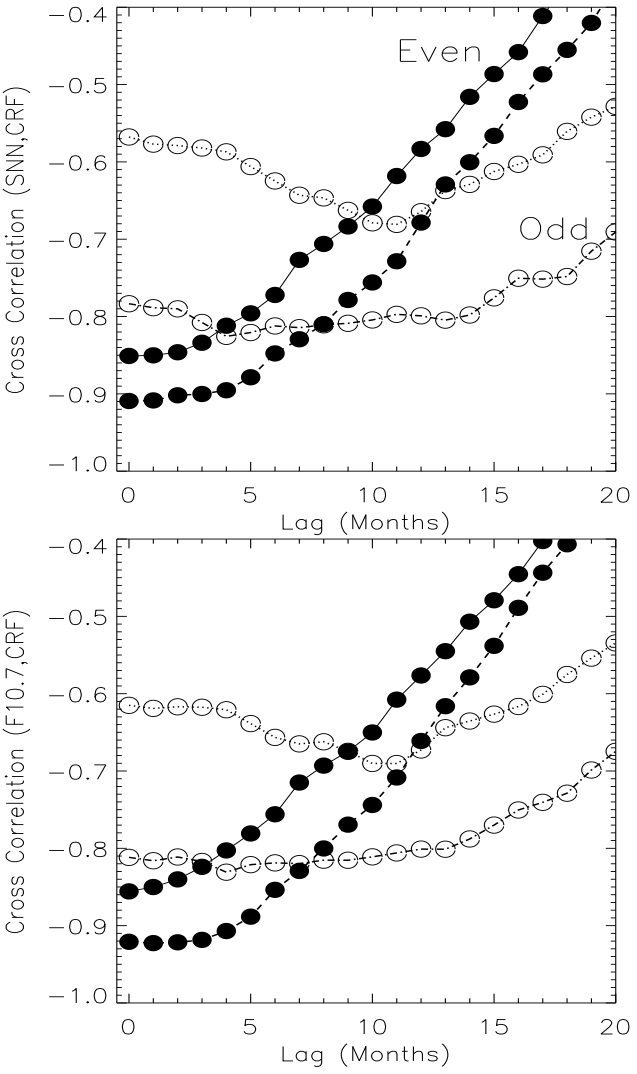

Fig. 2. Top. The running cross-correlation of CRF (McMurdo data) and F10.7 as a function of the lag (in months). Filled circles correspond to even cycles and open circles to odd ones. Bottom. The cross-correlation between CRF and SSN also as a function of the lag in months.

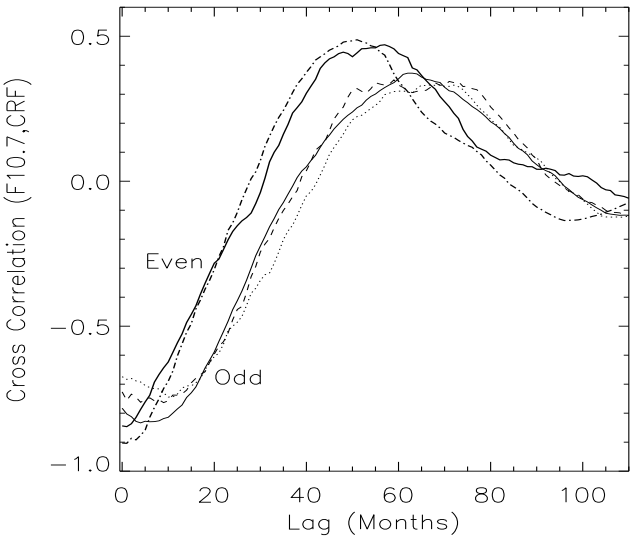

Fig. 3. The running cross-correlation of CRF Climax data and F10.7 as a function of the lag (in months). The bold continuous and dot-dashed lines are for even cycles and the thin continuous, dashed and dotted lines are for odd cycles, respectively.

larger time-lags than for even cycles. For odd cycles $C_{CRF-F10.7}$ is high and negative for time-lags up to ≈15 months. It reaches the largest negative value at ≈10–12-month lags. It remains at high values for ≈15-month time-lags. For even cycles the $C_{CRF-F10.7}$ at short lags (3–5 months) is larger than for odd ones but for larger lags it rapidly decreases.

2.2. *Histograms of Normalized Values*

We have made histograms of the F10.7, CRF and SSN data with the aim of comparing them with histograms of the CRF/F10.7 and CRF/SSN ratios.

The CRF, F10.7 and SSN data are normalized to unity by dividing each set by their own maximum value which, in the monthly averaged data of the Climax station, took place in 1987.17. For the F10.7 monthly data it occured in 1957.75 and for the SSN monthly data, in 1957.75. Further, we refer to the normalized values as CRF^1, $F10.7^1$ and SSN^1.

The F10.7 histograms for different cycles are similar to each other; all of them have an outstanding maximum at low fluxes and decrease as the flux increases. The data at the CRF histograms are somewhat spread but two weak maxima, whose positions on the distribution differ from one cycle to another but arise at about 0.88 and 0.98 of the normalized values, are observed.

We estimated the $CRF^1/F10.7^1$ and CRF^1/SSN^1 ratios and made the corresponding histograms. It should be noted that the histogram of the $CRF^1/F10.7^1$ ratio (Figure 4) is similar neither to the CRF histogram nor to that of the F10.7, neither shown in this figure. As shown by the continuous line (for $CRF^1/F10.7^1$) and by the grey shaded area (for CRF^1/SSN^1) of Figure 4, the maximum of occurrence, which is displaced from one cycle to another, is seen at the lowest values in the five cycles. It is worth noting that a shift took place between cycles 19 and 20 (going from lower to higher values). On the other hand, from cycles 20 to 22 the maximum gradually shifted to lower values.

The data of the CRF^1/SSN^1 histogram, for values larger than the maximum, are considerably more spread than those of $CRF^1/F10.7^1$. This is due to a

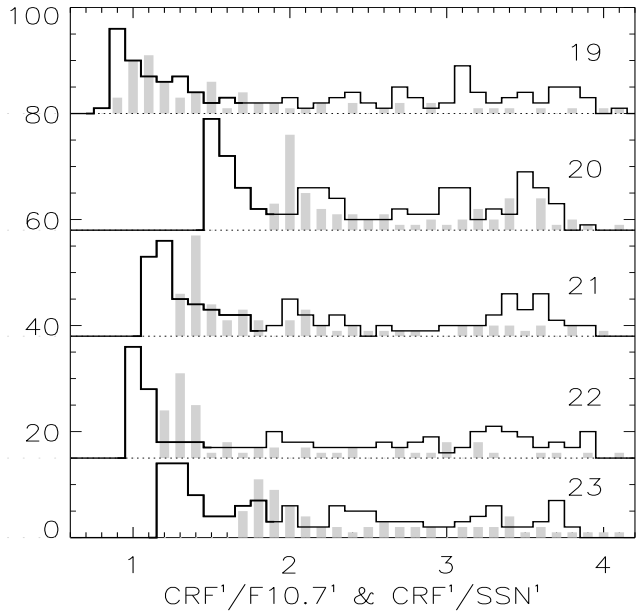

Fig. 4. Histogram of $CRF^1/F10.7^1$ (continous lines) and CRF^1/SSN^1 (grey shaded areas) ratios using CR Climax data. The values in the y-axis correspond to the frequency of occurrence for the lower plot. For the shifted histograms the frequency of occurrence has to be taken with respect to the horizontal line at the base of each plot.

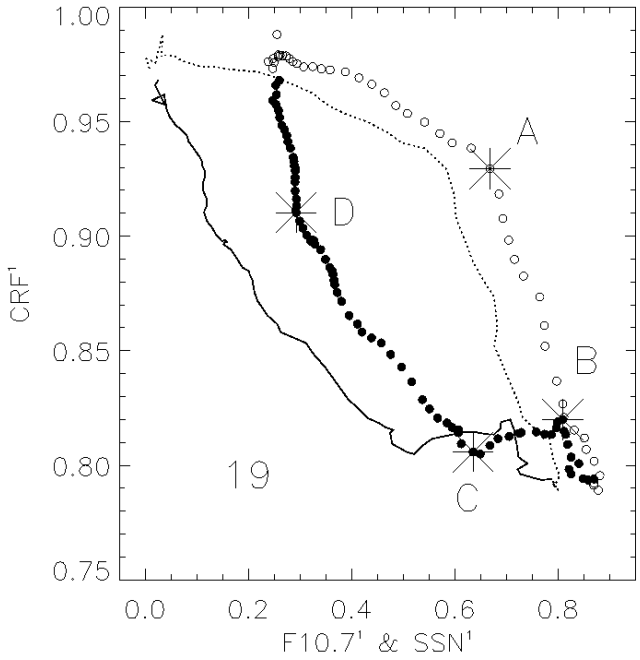

Fig. 5. The normalized cosmic ray flux (CRF^1) against the normalized fluxes at 10.7 cm ($F10.7^1$) for cycle 19. In the main text we refer to this kind of plot as hysteresis plot. Open circles correspond to the first part of the cycle and filled circles to the second part. The lines show the CRF^1 against the normalized sunspot number (SSN^1); the first part of the cycle is indicated with a dotted line and the second part with a continuous line. Asterisks, labelled with letters, denote the turnover points of the slope.

number of SSN low values that make the CRF^1/SSN^1 histograms extend beyond 100, while the $CRF^1/F10.7^1$ histogram has no values larger than 5.

2.3. *Scatter Plots of Normalized Values*

The CRF^1, $F10.7^1$ and SSN^1 are smoothed by averaging with a moving window of 10 data points length (10 months) and then plotted. The scatter plots of CRF^1 versus $F10.7^1$ are very similar to those of CRF^1 versus SSN^1 (Figures 5 and 6). As previously found (Bachmann & White 1994; Gupta et al. 2006; Singh et al. 2008) the plots show the hysteresis phenomenon between CRF and solar activity tracers and are further referred to as hysteresis plots.

In Figures 5 and 6 the hysteresis plots for cycles 19-23 are shown, empty circles are for the period from the beginning to the maximum of each cycle and filled circles for the period from the maximum to the end of the same cycle. The values for the beginning of each cycle appear at the upper-left of the plot. The data at the lower-right are observed near the maximum of each cycle. The data points draw a path that evolves in clockwise direction and becomes closed for the whole cycle.

As previously found (Gupta et al. 2006; Singh et al. 2008) there is a clear difference between odd and even cycles. At odd cycles there is almost no overlapping of data before (empty circles) and after (filled circles) the activity maximum. Only few values overlap around the data of the maximum of the cycle and the segment of the figure with empty circles is fully separated from that with filled circles. On the other hand, for even cycles the empty and filled circles overlap at various locations of the scatter plot. The behaviors of CRF^1 vs SNN^1 scatter plots (dotted and continuous lines in Figures 5 and 6) are very similar to those of CRF^1 vs $F10.7^1$.

The plot of two periodic functions on a Cartesian axis results in a Lissajous figure whose shape depends on the periods, the phase lag between the functions, and their amplitudes. Two functions of the same period and amplitude and either a zero- or 180-degree phase-lag would lead to a 45°- inclined straight line.

Figure 5 resembles the Lissajous figure for a $5/4\pi$ phase delay which is an ellipse tilted $-45°$, drawn in clockwise direction. The small loop is also similar to the Lissajous figure for the same phase delay. However, our loops are tilted about 20 degrees; also, the interpretation of the whole trajectory as a Lissajous figure is not straightforward, since to generate two loops traced in clockwise direction, the phase delay should be $5/4\pi$ for two different periods. This means that a phase delay of 5/8 T (with T, the period), would have to take

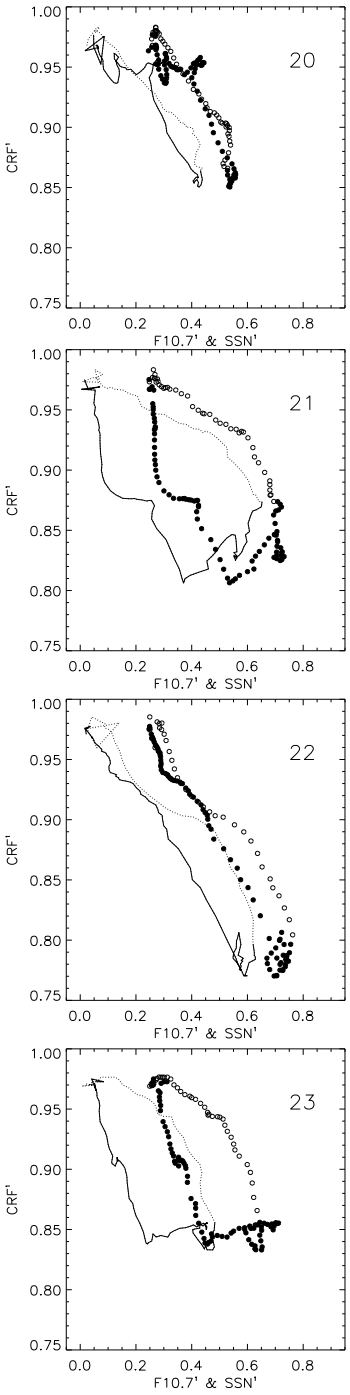

Fig. 6. Hysteresis plots of normalized fluxes for the 20–23 cycles. The signs and the lines are as in Figure 5. As for the 19 cycle, for 21 and 23 cycles the plot has different slopes at different times and the data for the first half of the activity cycle are fully separated from the data for the second half. Different from odd cycles, in cycles 20 and 22 the slopes of CRF^1 vs $F10.7^1$ and CRF^1 vs SSN^1 are similar at different times of the activity cycle.

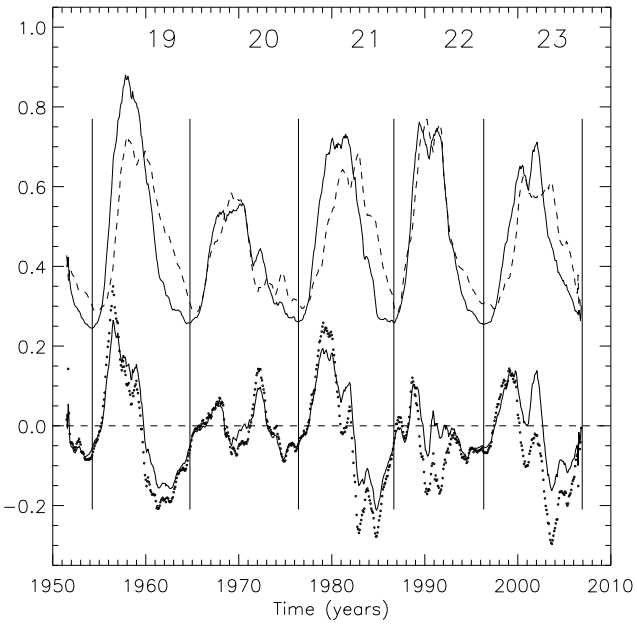

Fig. 7. The dashed line represents the smoothed CRF^{inv} time profile and the thin continuous line (in the upper part) the $F10.7^1$ one. The bold continuous line (in the lower part) is the difference of the upper curves ($F10.7^1$- CRF^{inv}) referred to as DNF. Dots represent the difference SSN^1-CRF^{inv} referred to as DNS. The SSN^1 time profiles for the odd cycles are similar to each other, but shifted to lower values from one cycle to the next.

place for both, the 11-year period and also for the 1.5-year period, which would require 6.9-year and 0.94-year delays, respectively. With such different time delays, a coincident same phase delay is not easy to explain.

2.4. *Inverted CRF Time Curve*

An inverted curve of the cosmic ray flux (CRF^{inv}) was estimated by using a linear function so that $CRF^{inv} = a + b * (1 - CRF^1)$, with a and b constants, thus obtaining the inverted curve of CRF (further referred to as CRF^{inv}). The constants were selected so that the CRF^{inv} curve (dashed line in Figures 7 and 8) has both a similar amplitude and background level as the $F10.7^1$ curve (continuous line).

The CRF^{inv}, $F10.7^1$ and SNN^1 are smoothed by averaging each with a moving window of 10 data points. The smoothed values are used to compute $F10.7^1$-CRF^{inv} and also SSN^1-CRF^{inv}, which are further referred to as difference with normalized flux (DNF) and difference with normalized sunspots number (DNS), respectively. Both are plotted in the bottom of Figures 7 and 8, DNF is denoted with a bold continuous line and DNS with dots. We consider that the fit of CRF^{inv} to $F10.7^1$ is good when for a given cycle the negative and positive values of the DNF are approximately equally distributed at both sides of the zero line.

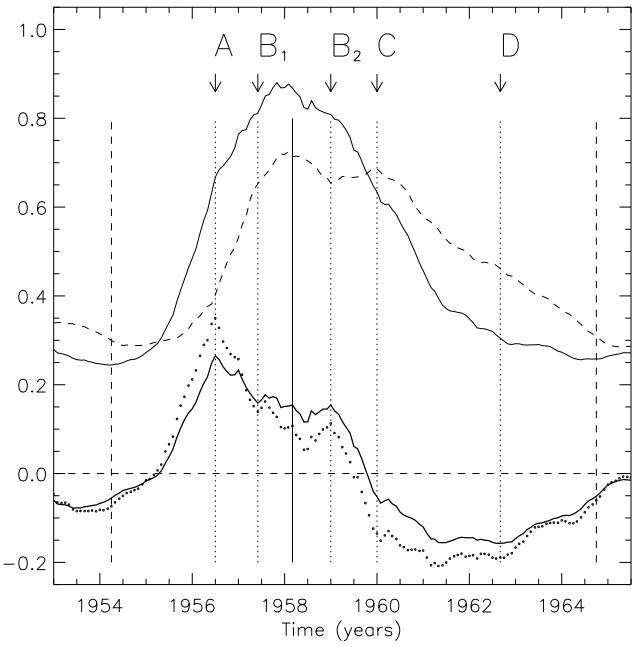

Fig. 8. Time profiles for cycle 19. The lines and signs are as in Figure 7,the dashed line represents the CRF^{inv} and thin continuous the $F10.7^1$ (in the upper part), the bold continuous line (in the lower part) is for DNF, the difference $F10.7^1$-CRF^{inv} and circles for DNS (SSN^1-CRF^{inv}). The letters indicate the turnover points shown in Figure 5. The vertical dotted lines indicate the minima and the continuous vertical line, the maximum of the activity cycle.

A CRF^{inv} curve obtained with a pair of a and b values may fit well to a given time segment of the $F10.7^1$ curve of Figure 7, but at other segments may not fit as well. This means that, by varying the a and b constants, one may improve the fit to a given cycle, but make the fit worse for other cycles. In general, the behavior of DNF for the whole period is similar when fitting CRF^{inv} to $F10.7^1$ for different cycles and the DNF curve only shifts up or down from one case to another.

Before the activity maximum of each odd cycle an increase and after it a decrease of DNF and DNS are observed. These variations in the first half of the activity cycle form a sharp feature with a maximum in the DNF and DNS curves (Figure 7). Also, in the DNF and DNS curves of odd cycles, a deep decrease down to negative values and after that an increase form a minimum during the second half of the activity cycle.

2.4.1. *Two maxima at the activity maximum*

It is worth paying attention to two maxima at the high activity phase of F10.7 which may be seen at $F10.7^1$ and CRF^{inv} in Figure 7, and that also appear at SNN^1 (not shown in this figure). The amplitude of these maxima changes little at SSN^{inv} from one cycle to another, leading the DNS shape to be similar in the three odd cycles. However, at $F10.7^1$ the second maximum (M_2) gradually grows from one cycle to the next.

In cycles 19 and 21, the DNF goes from large positive values at the first part of the cycle to large negative values at the second part. In cycle 23 the situation is similar but M_2 at F10.7 is higher in cycle 23 than in previous cycles and leads to a maximum of DNF at the high activity phase making its shape different from the other odd cycles (Figure 7). Also, the negative part at the end of cycle 23 is deeper at DNS than at DNF, particularly in cycle 23. Livinstgon et al. (2012) found that in cycle 23 the SSN decreases compared to F10.7. This result agrees with the distinct DNF and DNS behavior found here. It seems that further studies of the relation between the two high activity maxima could give some insight into the cosmic ray flux modulation.

2.4.2. *Phases in the hysteresis plots and in the $F10.7^1$-CRF^{inv} difference*

Point A in Figure 5 is the earliest turnover point, the first from the beginning of the cycle. We could consider as phase 1 the period between the beginning of the cycle and this point. At this time the CRF varies little with respect to the F10.7 and SSN variations. Point *A* in Figure 5 corresponds to the time, also denoted by *A* in Figure 8, when the growth of F10.7 (upper continuous line) slows down. On the other hand, at about this point, the CRF (dashed line, also in Figure 8) turns to a slightly faster growing behavior. As a result, a maximum of the DNF time curve (continuous bold line) takes place. Phase 2 occurs at the period between points A and B. The variation of CRF is larger than for F10.7 and SSN. At this period the DNF time-curve decreases in agreement with a large variation of CRF with respect to F10.7. The slope at phase 2, is near −1. This indicates that the correlation is high.

Phase 3 is particular because it traces a path that, in about 1.5 years, departs from point B (at the time B_1 in Figure 8) and returns to it (at the time B_2), forming a small loop. The loop apex, opposite to point B in Figure 5, occurs close to the time of the maximum of the activity cycle. At this phase the DNF curve (continuous bold line in Figure 8) is almost flat with the time of the maximum of activity (continuous vertical line) located close to the midpoint of this interval.

Around the beginning of the decreasing phase of the activity cycle, between points B and C (phase 4), the slope of the hysteresis plot of Figure 5 becomes close to zero. This means, that the correlation considerably decreases. It is worth mentioning that at this phase the slope is positive (Figures 5 and 6).

In the first half of phase 6 the DNF curve (lower continuous line in Figure 8) shows a decrease slower than that of the previous phase and in the second half the DNF curve is almost constant. In the last phase of the cycle, i.e. between point D and the apex at the

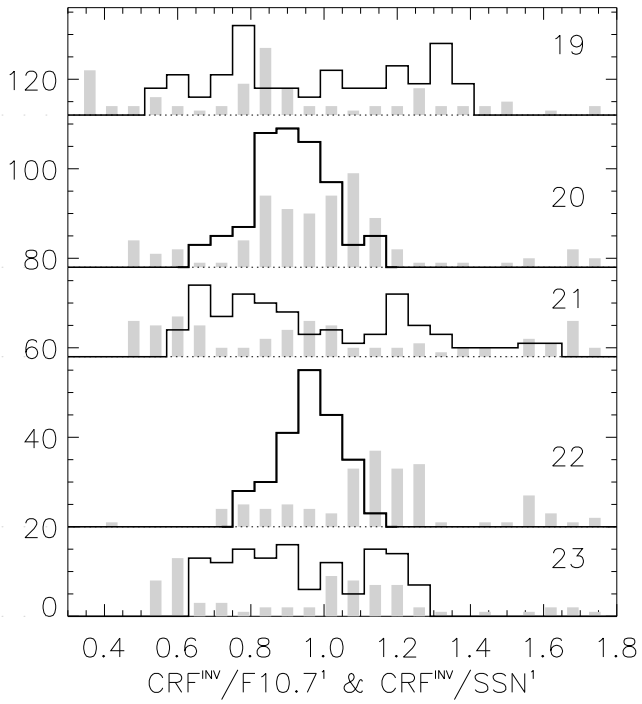

Fig. 9. Histogram of $CRF^{inv}/F10.7^1$ (continous lines) and CRF^{inv}/SSN^1 ratios (grey shaded areas) using CR Climax data. In the y-axis the frequency of occurrence is given for the lower plot. For the shifted histograms the frequency of occurrence has to be taken with respect to the horizontal line at the basis of each plot. It may be seen that for even cycles the $CRF^{inv}/F10.7^1$ values are clumped near unity.

beginning-end of the cycle, in the hysteresis plot the correlation again is high at cycle 19 but not in cycles 21 and 23.

2.4.3. *Histograms of the CRF^{inv}/ F10.7^1 and CRF^{inv}/SSN^1 ratios*

The histograms of the $CRF^{inv}/F10.7^1$ ratio (continuous line) and of the CRF^{inv}/SSN^1 ratio (shaded areas) are shown in Figure 9. The $CRF^{inv}/F10.7^1$ histogram for even cycles the maximum lies around unity, with the bulk of data concentrated close to it. On the other hand, in odd cycles the distributions show a weak accumulation of values on both sides of unity.

In the CRF^{inv}/SSN^1 histograms, for even cycles, the number of values around unity is considerably less than for $CRF^{inv}/F10.7^1$, with no prevailing maximum. For odd cycles the values are more spread out, with the maximum near unity, but the CRF^{inv}/SSN^1 histograms do not show the accumulation at their sides, as they do for the $CRF^{inv}/F10.7^1$ histogram.

3. DISCUSSION

The results found for CRF with respect to F10.7 and with respect to SSN confirm results previously reported. Also, new aspects of the CRF variations that could be due to modulation by the Sun and another whose origin is not clear, are found and analyzed below.

It is remarkable that the behavior of the maximum in the $CRF^1/F10.7^1$ histogram does not depend on the polarity of the cycles. Such a behavior in the relation of CRF and tracers of the activity cycle has not been previously reported.

The present hysteresis plots give new details into the different behaviors of odd and even cycles. Also, it is worth noting that they reveal details of the relation of CRF with F10.7 and SSN at different times of the solar activity cycles. This is clear from the hysteresis plots for odd cycles, which contain features revealed as different slopes for different times of the activity cycle and a small loop. The loop had been roughly drawn previously by Singh et al. (2008) but not reported as a particular feature of the hysteresis plot. The change of the slope indicates that the correlation between CRF and F10.7 (and likewise for CRF and SSN) varies with the solar cycle and suggests that the turnover points (A, B, C, and D in Figure 5) could be the milestones of at least seven different phases in the relation between CRF with F10.7 and SSN. The hysteresis plots like CRF^1 vs $F10.7^1$ could even be used to determine the beginning, the maximum and the end of a cycle of activity for an odd cycle.

We recall that $DNF=F10.7^1-CRF^{inv}$ and $DNS=SSN^1-CRF^{inv}$ (Figure 7). It may be seen that the DNF shapes for odd cycles remain similar to each other but they are shifted down from one cycle to the next, i.e, the $F10.7^1-CRF^{inv}$ difference goes to lower values from one cycle to the next and the same occurs for DNS. This can be interpreted as a result of an increasing CRF along the time of the five cycles here studied. An increase of the cosmic ray flux for a half year period between 2008 and 2009 was observed at the Irkustk station (Kravtsova & Sdobnov 2011). This increase could be part of the longer period of cosmic ray flux increase here observed.

As seen above, the $CRF^{inv}/F10.7^1$ histogram clearly reveals the aggregating character of the data around unity (Figure 9). This means that for even cycles the CRF^{inv} values at a given time are closely related to the $F10.7^1$ values at the same time; therefore, the $CRF^{inv}/F10.7^1$ ratios do not extend far from a given central value. On the other hand, for odd cycles, the $CRF^{inv}/F10.7^1$ values do not have a tendency to clump around unity but show a weak accumulation at both sides, which indicates that the CRF^{inv} does not have the tendency to closely follow the behavior of F10.7 in these cycles (as also seen the hysteresis plots, where the slope varies with phase).

Different from the above situation, the CRF^{inv}/SSN^1 histograms show neither an out-

standing maximum around unity for even cycles nor a slight accumulation at both sides of it for odd cycles. From the different behaviors of the $CRF^{inv}/F10.7^1$ and CRF^{inv}/SSN^1 histograms (Figure 9), in particular the accumulation of the data around unity, it seems more convenient to use F10.7 rather than SSN data. The failure of SSN to trace a distribution with clear maxima could partially be due to their low values at some phases of activity.

The hysteresis plots and DNF and DNS, in particular for odd cycles, seem to reveal the modulation effects on cosmic ray flux of different phenomena, whose role varies with the activity cycle. Among the phenomena responsible for CR modulation, we can consider at least three different types: (1) CR of solar origin, that arise at AR during flares, whose flux varies with the activity cycle, with the peculiarity that it can suddenly increase the CRF at transient events, in time-scales of hours, such as in the initial phase of Forbush; (2) Near Sun Heliosphere phenomena such as coronal mass ejections (CME) and corotating shocks (CS) that during their propagation in the interplanetary medium (IPM) inhibit the CR transport; and (3) Far away phenomena, near the frontiers of the heliosphere, such as the storage of charged particles at the heliosheath. Far-away regions in the heliosphere may play an important role in the transport of charged particles (Florinski 2011), and as found by Luo et al. (2011) the charges can expend considerably more than a year there in a random walk.

The CR modulation takes place at different timescales (Potgieter 2008; Usoskin et al. 1997) but also, variations due to conditions outside the heliosphere can be considered for long-term variations (Scherer et al. 2006). The CRF also suffers the influence of the local interstellar medium (Usoskin et al. 2005; Yeghikyan & Fahr 2004), which could be not evident during high solar activity periods but could become more clear during quiet activity periods.

The DNF and DNS curves (Figure 7), and in particular the maxima and minima above mentioned (observed near the minimum of the activity cycle), go to lower values from one cycle to another. This indicates that for the time period of the five cycles analyzed, which is larger than half a century, the cosmic ray flux increased in relation to both the flux at 10.7 cm and the sunspot number. Causes of this increase external to the heliosphere could be, for instance time-varying sources and magnetic field or cosmic ray flux gradients inside which the Solar System is moving.

The F10.7 parameter shows that it is suitable to study the CRF modulation by the solar activity. Further work to compare the CRF with the flux at other microwave frequencies and also with the spectral index of the radio emission spectrum could probably give a deeper insight into the modulation phenomenon.

4. CONCLUSIONS

In the $CRF^1/F10.7^1$ histograms, a maximum that shifts from one cycle to another was found. The shift does not seem to depend on the polarity of the cycle.

The histeresis plots of CRF^1 vs $F10.7^1$ show a clear difference between odd and even cycles. For odd cycles they generate a closed path with clearly separated trajectories for the increasing and decreasing phases of activity. The variations of the slopes for CRF^1 vs $F10.7^1$ and also the subtraction $F10.7^1 - CRF^1$ point to the possibility of at least seven phases of the CRF to F10.7 relation.

In the $CRF^{inv}/F10.7^1$ histograms of even cycles, a data accumulation takes place around unity, and for odd cycles two weak maxima are seen at both sides of unity.

For SSN the results are similar to those of F10.7 but for the CRF^{inv}/SSN^1 histograms they differ, since for CRF^{inv}/SSN^1 no maxima are observed, showing that the above behavior could be identified only with the use of the 10.7 cm data.

We acknowledge the Bartol Research Institute neutron monitor program supported by the United States National Science Foundation under grants ANT-0739620 and ANT-0838839, and by the University of Delaware Department of Physics and Astronomy and Bartol Research Institute, for the use of McMurdo Neutron Monitor data; also, the New Hampshire University, "National Science Foundation Grant ATM-0339527" for the use of CLIMAX Neutron Monitor data; the SIDC-team, World Data
Center for the Sunspot Index, the Royal Observatory of Belgium, Ringlaan 3, 1180 Brussel, Belgium, the International Sunspot Number, Monthly Report on the International Sunspot Number, online catalogue of the sunspot index: `http://www.sidc.be/sunspot-data/`, for the use of Sunspot data from 1951 to 2006; and the Penticton Dominion Radio Astrophysical Observatory, of the National Research Council of Canada for the use of the solar flux data at 10.7 cm.

REFERENCES

Akhmedov, S. B., Gelfreikh, G. B., Bogod, V. M., & Korzhavin, A. N., 1982, Solar Physics, 79, 41

Aschwanden, M. J. 2005, Physics of the Solar Corona. An Introduction with Problems and Solutions (2nd ed. Springer-Verlag, Berlin)

Bachmann, K. T., & White, O. R. 1994, Solar Physics, 150, 347

Cliver, F.W., & Ling, A.G. 2001, ApJL, 551, L189

Florinski, V. 2011, Adv. Space Res., 48, 308

Gupta M., Mishra, V.K., & Mishra, A.P. 2006, Indian J. Radio Sp. Phys. 35, 167
Heber, B., Fichtner, H., & Scherer, K. 2006, Space Science Reviews, 125, 81
Kravtsova, M.V., & Sdobnov, V. E. 2011, Proc. 32nd ICRC, Beijing, China, 11, 228
Livingston, W., Penn, M.J., & Svalgaard, L. 2012, ApJL, 757, L8
Luo, X., Zhang, M., Rassoul, H. K., & Pogorelov, N. V. 2011, ApJ, 730, 13
Potgieter, M.S. 2008, Journal of Atmospheric and Solar-Terrestrial Physics, 70, 207
Scherer, K., et al. 2006, Space Sci. Rev., 127, 327
Singh, M., Singh, Y. P., Badruddin, 2008, Journal of Atmospheric and Solar-Terrestrial Physics, 70, 169
SIDC-team, Monthly Report on the International Sunspot Number, online catalogue 1951–2006, `http://www.sidc.be/sunspot-data/`.
Usoskin, I.G., Kovaltsov, G.A., Kananen, H., Mursala, K., & Tanskanen, P. 1997, Proc. 25th ICRC, Durban, South Africa, 2, 201
Usoskin, I.G., Mursula, K., Kananen, H., & Kovaltsov, G.A. 2001, Adv.Space Res., 27, 571
Usoskin, I.G., Alanko-Yuotari, K., Kovaltsov, G.A., & Mursala, K. 2005, J. Geophys. Res. 110, A12108
Yeghikyan, A., & Fahr, H. 2004, A&A, 415, 763

Xi Luo: SIGMA Weather Group, State Key Laboratory of Space Weather, Center for Space Science and Applied Research, Chinese Academy of Sciences, Beijing 100190, China (xluo@spaceweather.ac.cn).
J. Eduardo Mendoza-Torres: Instituto Nacional de Astrofísica, Óptica y Electrónica, Apdo. Postal 51 y 216, Puebla 72000, Mexico (mend@inaoep.mx).
Humberto Salazar: Facultad de Ciencias Físico-Matemáticas, Benemérita Universidad Autónoma de Puebla, Puebla 72592, Mexico (hsalazar@fcfm.buap.mx).